JACS
JOURNAL OF THE AMERICAN CHEMICAL SOCIETY

Article

pubs.acs.org/JACS

Protein Detection by Nanopores Equipped with Aptamers

Dvir Rotem,[†,§] Lakmal Jayasinghe,[‡] Maria Salichou,[†] and Hagan Bayley[†,*]

[†]Department of Chemistry, University of Oxford, Oxford, OX1 3TA, United Kingdom

[‡]Oxford Nanopore, Edmund Cartwright House, Oxford Science Park, Oxford OX4 4GA, United Kingdom

Supporting Information

ABSTRACT: Protein nanopores have been used as stochastic sensors for the detection of analytes that range from small molecules to proteins. In this approach, individual analyte molecules modulate the ionic current flowing through a single nanopore. Here, a new type of stochastic sensor based on an αHL pore modified with an aptamer is described. The aptamer is bound to the pore by hybridization to an oligonucleotide that is attached covalently through a disulfide bond to a single cysteine residue near a mouth of the pore. We show that the binding of thrombin to a 15-mer DNA aptamer, which forms a cation-stabilized quadruplex, alters the ionic current through the pore. The approach allows the quantification of nanomolar concentrations of thrombin, and provides association and dissociation rate constants and equilibrium dissociation constants for thrombin·aptamer interactions. Aptamer-based nanopores have the potential to be integrated into arrays for the parallel detection of multiple analytes.

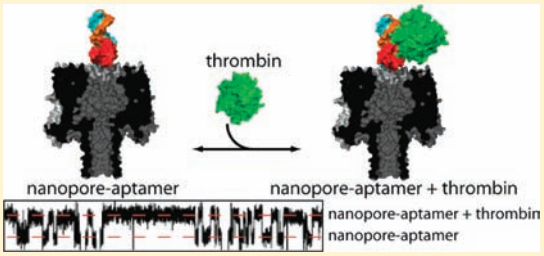

INTRODUCTION

Stochastic sensors based on nanopores are under intense investigation.[1−7] In this approach to single-molecule detection, the reversible interaction of an analyte with a pore alters the current flowing through it, which is carried by aqueous ions. The change in the current amplitude and the mean dwell time of the analyte reveal the analyte's identity, while the number of events per unit time yields the analyte concentration.[2] Modified pores that bind specific analytes or families of analytes are especially useful for stochastic detection. In this regard engineered protein pores, notably staphylococcal α-hemolysin (αHL), have been most effective.[2] The αHL pore has been used to detect metal ions,[8−10] small molecules,[11,12] reactive molecules,[13] DNA,[14] and proteins.[15−18]

Because proteins are too large to bind within the lumen of the αHL pore, various approaches have been taken to transmit binding events occurring outside the pore to the interior so that the ionic current is altered. In one example, one end of a polymer was covalently attached within the αHL pore, while a ligand was attached the other end, which was free to explore the nearby buffer. The reversible binding of proteins in either the cis or trans solution (Figure 1) was detected as a dampening of the fluctuations of the polymer within the pore, manifested as decreased current "noise".[15] Lectins have been detected after the attachment of disaccharides near the cis entrance of the pore. In this case, binding resulted in a decrease in the ionic current.[16] Protein kinases have been detected after equipping the αHL pore with a protein kinase inhibitor peptide, attached chemically[17] or by using a genetic insert,[18] in both cases near the trans entrance. In the first case, the binding of a kinase subunit caused a current block.[17] In the second case, kinase binding caused both a current block and diminution of current noise arising from movement of the insert near the entrance to the pore.[18]

In the present work we describe a different approach for protein detection by stochastic sensing that provides a flexible means to change the detecting ligand. First, a short DNA oligonucleotide is covalently attached to a cysteine residue near the entrance of the nanopore through a disulfide bond (Figure 1a);[14,19,20] the oligonucleotide acts as an adapter to which various nucleic acid ligands can be coupled by duplex formation.[14,19,20] One class of nucleic acid ligands encompasses aptamers, which are DNA or RNA oligonucleotides that adopt three-dimensional structures capable of binding various analytes, including small molecules, proteins, and even cells.[21,22] Aptamers have been used as biosensor components[23] or as therapeutic agents.[24]

Aptamers are selected *in vitro* by using SELEX (systematic evolution of ligands by exponential enrichment).[25,26] The starting point for SELEX is a large library of randomized oligonucleotide sequences (>10^{13}). A selection and amplification process is repeated until oligonucleotides with high affinity for the target have been obtained.[25,26] In the present work, thrombin has been chosen as a target analyte. Its interactions with various aptamers have been detected previously by using various analytical devices (e.g., capillary electrophoresis, surface plasmon resonance, MALDI mass spectrometry[27]), none of which operate at the single molecule level.

Ding and colleagues attached multiple aptamers near the mouth of a narrow glass micropipet and were able to record a series of individual but irreversible binding events for both IgE and ricin.[28] Here, we use a 15-mer DNA aptamer,[29] which

Received: November 18, 2011
Published: January 9, 2012

   dx.doi.org/10.1021/ja2105653 | J. Am. Chem.Soc. 2012, 134, 2781−2787

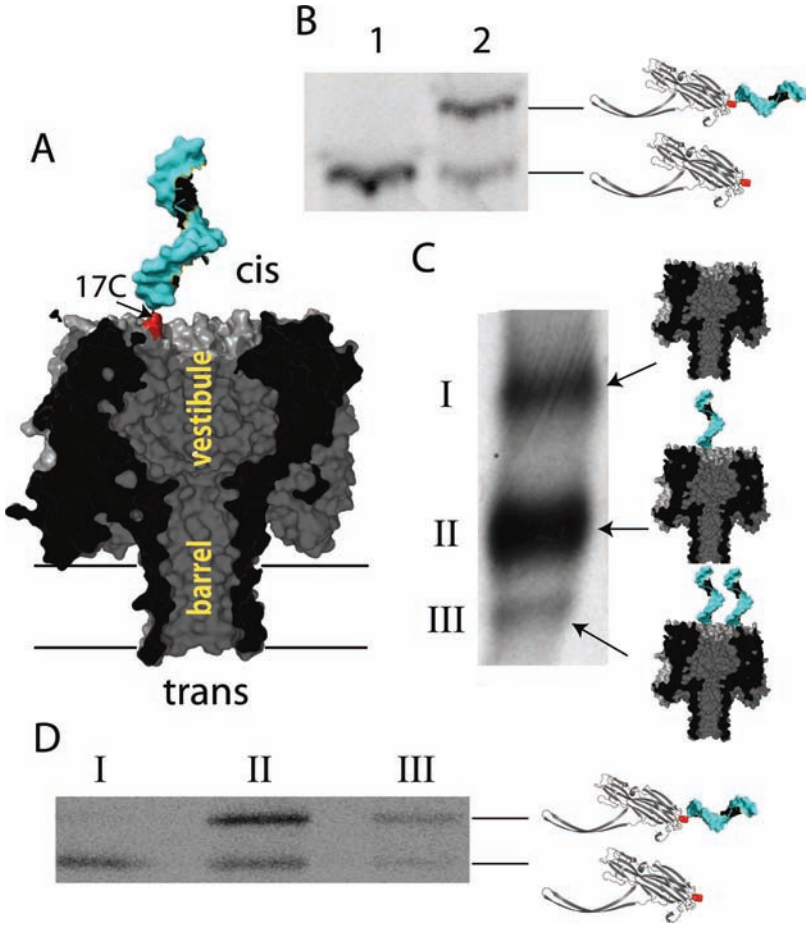

Figure 1. Attachment of a single DNA oligonucleotide to the αHL pore. (a) Cross-section of a model showing an αHL pore chemically modified with a single DNA oligonucleotide. The oligonucleotide is attached by a hexamethylene linker and a disulfide bond to Cys-17 of a single genetically engineered subunit within a heptameric αHL pore. The model was made with PyMOL software (www.pymol.org) based on the pdb files 7AHL (αHL, gray) and 3IAG (ssDNA, light blue). (b) Autoradiogram of an SDS-polyacrylamide gel (Criterion XT Precast Gel, 10% acrylamide) showing αHL N17C monomers before (lane 1) and after (lane 2) reaction with the activated oligoA oligonucleotide. Schematic representations of αHL N17C monomers with and without an attached oligoA are shown. (c) Autoradiogram of an SDS-polyacrylamide gel (Tris.HCl gel, 5% acrylamide) showing unheated samples of αHL heptamers formed on rabbit red blood cell membranes with a mixture of ^{35}S-labeled N17C-oligoA monomers and excess unlabeled WT monomers. Schematic representations of αHL pores with 0, 1, or 2 attached oligoA oligonucleotides are shown. (d) Autoradiogram of an SDS-polyacrylamide gel of polypeptides found in the bands from part c. The samples were extracted from the first gel, denatured (10 min, 95 °C in XT sample buffer, Bio-Rad) and run in second gel (Criterion XT Precast Gel, 10% acrylamide). Note that the mobility of heptameric αHL in SDS-polyacrylamide gels is increased after modification with DNA, while the mobility of monomers is decreased by DNA attachment.

forms a cation-stabilized quadruplex[30−32] that binds thrombin reversibly and is therefore suitable for continuous real-time sensing. Because it is a simple matter to change the oligonucleotide that is hybridized to the adapter, we could rapidly compare the properties of various versions of the aptamer. We suggest that the approach might be applied to the fabrication of sensor arrays.

RESULTS AND DISCUSSION

DNA Oligonucleotide Attachment to the αHL Nanopore. An 18-mer DNA oligonucleotide (oligoA) was attached to the αHL N17C monomer through a disulfide bond to Cys-17. Cys-17 is the only cysteine residue in this polypeptide since the wild-type αHL contains no cysteine residues. About 70% of the N17C subunits were derivatized as determined by the mobility shift in SDS-polyacrylamide gels (Figure 1b). The modified N17C monomers were mixed with excess WT monomers and assembled in the presence of rabbit red blood cell membranes to form heteroheptameric pores, which are stable toward SDS.[33] The pores with more oligonucleotides migrated faster (Figure 1c). αHL $WT_6$17C_1 heteromeric pores with oligoA attached near the cis entrance (Figure 1a) were extracted from the gel (band II, Figure 1c). Previous results suggest that monomers with additional negative charge usually migrate more slowly in SDS gels, while heptamers with additional negative charge usually migrate more rapidly.[14,33] Although there is no simple explanation of this finding, the present results are consistent with the phenomenon. On the basis of SDS-PAGE of denatured pores (lane II, Figure 1d) and the properties of the pores during single-channel recording (see below), it was concluded that a single copy of oligoA was attached to a large majority of the pores recovered from band II ($WT_6$17C-oligoA_1). The underivatized N17C subunits in band II must represent subunits from which DNA has become detached or N17C from $WT_5$17$C_1$17C-oligoA_1, which would migrate to the same position. In the following, we assume that $WT_5$17$C_1$17C-oligoA_1 has the same electrical

dx.doi.org/10.1021/ja2105653 | J. Am. Chem.Soc. 2012, 134, 2781−2787

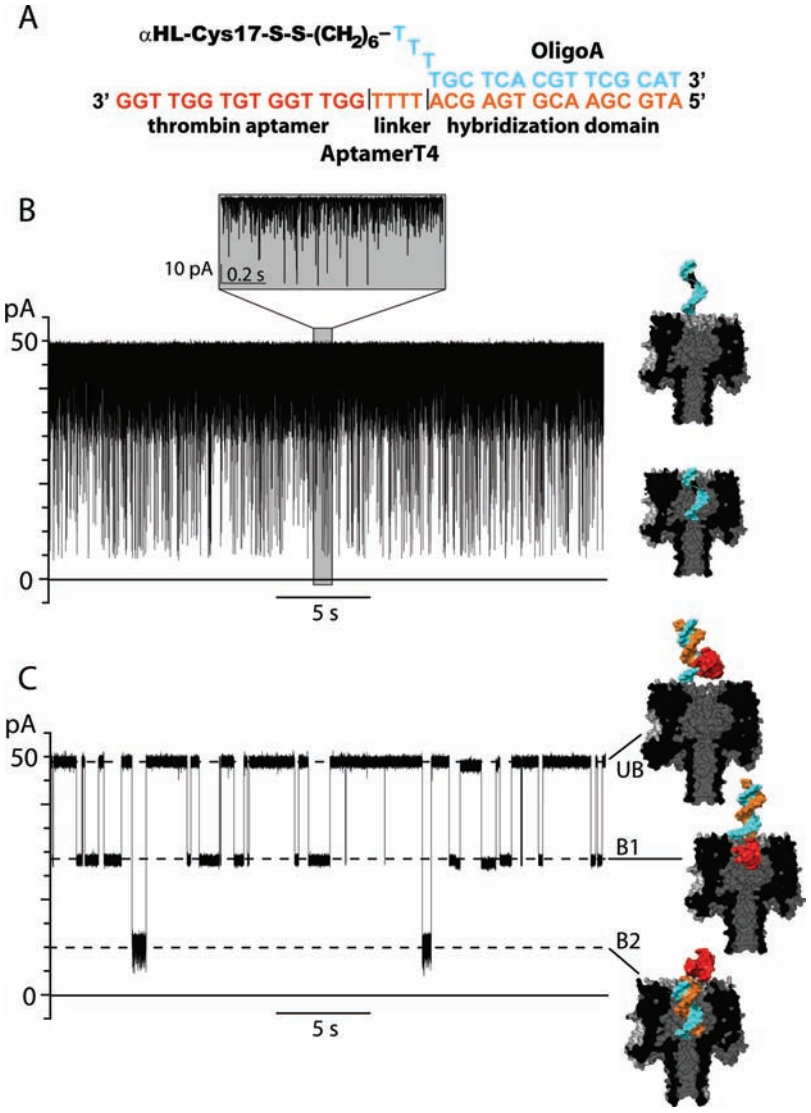

Figure 2. αHL pore with a thrombin aptamer attached by DNA hybridization. (a) The DNA duplex formed between oligoA and aptamerT4. (b, c) Representative single-channel recordings from the αHL-oligoA$_1$ pore (b) before and (c) after hybridization to aptamerT4. The measurements were performed in 1 M KCl, buffered with 10 mM Tris.HCl, pH 7.2, at +50 mV. The traces were filtered at 1 kHz. The models are based on pdb files 7AHL (αHL, gray), 3IAG (dsDNA, light blue and orange), and 148D (thrombin aptamer, red). Before hybridization to the DNA duplex, the DNA adapter moves in and out of the pore creating short, frequent blocking events as seen in part b. After hybridization of the aptamer, two blockade levels are observed, B1 and B2, as shown in part c. The B1 level is generated by movement of the quadruplex domain into the vestibule of the pore, while the B2 level arises from the insertion of the dsDNA segment into the pore (see the text).

properties as WT$_6$17C-oligoA$_1$, and refer to them collectively as αHL-oligoA$_1$.

Aptamer Hybridization to the DNA Adapter. Single-channel recordings at +50 mV of the unhybridized αHL-oligoA$_1$ pore showed short and frequent current blockades (Figure 2b). These events represent transient movements of oligoA into the pore. As the applied potential was increased, the dwell times of these events increased, and eventually (at above +100 mV) oligoA was permanently located inside the pore (Figure S1).

AptamerT4, which includes (5′ to 3′) a complementary sequence to oligoA (15 nt), a thymine linker (4 nt), and a thrombin-binding domain (15 nt) (Figure 2a), was hybridized to the oligoA adapter of αHL-oligoA$_1$ before the protein was added to the cis chamber. With hybridized aptamerT4, two blockade levels were observed at +50 mV: B1 (43 ± 1% current block, n = 7) and B2 (76 ± 2% current block, n = 7) (Figure 2c, Table 1). Various experiments were carried out to identify the sources of current block. Single-channel recording of αHL pores that were directly coupled to a thiolated thrombin aptamer showed only blocking events with a current level

Table 1. Transitions between Current Levels in αHL-oligoA$_1$·AptamerT4 Pores[a]

current level B1 % block: 43 ± 1%		current level B2 % block: 76 ± 2%	
transition	rate (s^{-1})	transition	rate (s^{-1})[b]
UB to B1	0.49 ± 0.22	UB to B2	0.18 ± 0.19
B1 to UB	2.1 ± 0.6	B2 to UB	7.6 ± 14.5

[a]The measurements were made in 1 M KCl, 10 mM Tris.HCl, pH 7.2, at +50 mV. Values are the mean ± s.d. (n = 7). [b]The rate of the transitions UB to B2 and B2 to UB were highly diverse: UB to B2, 0.05−0.58 s^{-1}; B2 to UB, 0.7−40 s^{-1} (Figure S4).

dx.doi.org/10.1021/ja2105653 | J. Am. Chem.Soc. 2012, 134, 2781−2787

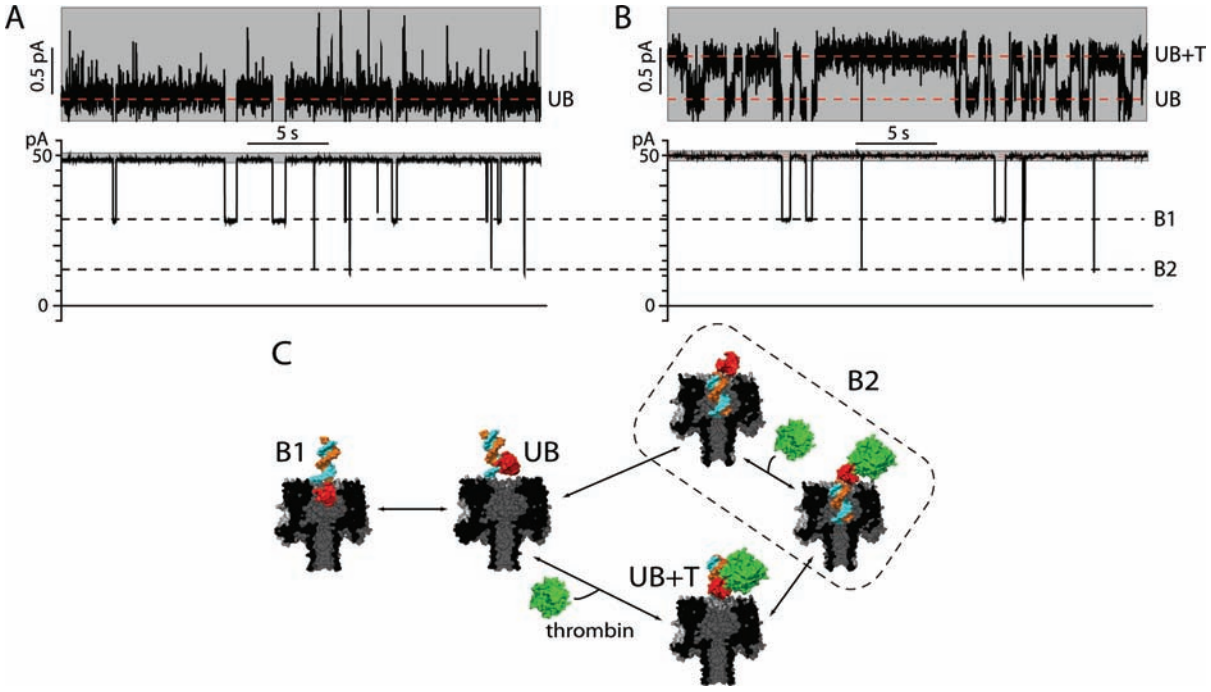

Figure 3. Detection of the interactions between thrombin and aptamerT4. Representative single-channel recordings of αHL-oligoA_1·aptamerT4 (a) before and (b) after the addition of 80 nM thrombin (final concentration) to the cis chamber. The measurements were performed in 1 M KCl, buffered with 10 mM Tris.HCl, pH 7.2, at +50 mV. In the presence of thrombin, a new elevated current level (UB+T) was observed and the frequency of the B1 blockades was reduced. The upper panels are enlargements of the gray boxes in the lower panels. The traces were filtered at 50 Hz. (c) A kinetic model for the transitions between the various currents levels observed in the presence of thrombin. The models are based on pdb files 7AHL (αHL, gray), 3IAG (dsDNA, light blue and orange), 148D (thrombin aptamer, red), and 1HUT (thrombin and thrombin·aptamer complex, green and green plus red, respectively).

similar to B1 (39 ± 2%, n = 4; Figure S2). This suggests that the B1 level is generated by insertion of the aptamer's quadruplex into the pore vestibule. The result is consistent with the finding of Shim and colleagues who showed that a free thrombin aptamer can enter the vestibule of the αHL pore and partially block the ionic current.[34,35] By contrast, when oligonucleotides that contained only a hybridization domain (Figure S3a), or contained a hybridization domain and a 19-mer extension that cannot form a quadruplex (Figure S3b), were hybridized to αHL-oligoA_1, blocking events with current levels similar to B2 were observed. This suggests that B2 represents the insertion of the double-stranded portion of the hybridized structures into the pore vestibule. The rate of the transitions to and from current level B2 varied greatly from pore to pore, regardless of which oligonucleotide was hybridized to the adapter (Figure S4), and we have no explanation for this phenomenon, other than the unpersuasive supposition that the pore structures differ subtly. The amplitude of the B2 blockade, and the amplitudes and kinetics of the other blockades were not subject to this kind of variation. Importantly, the rates of the transitions to and from B2 did not affect thrombin detection by the aptamer (see below).

The frequency of the transitions to level B1 (aptamer insertion into the pore) and the dwell time in this level increased as the applied potential was raised (Figure S5). At high positive potentials (e.g., +80 mV, Figure S5), a new current level was observed for a short time (94% current block, arrow, Figure S4). Subsequently, fast transitions to and from another new current level (89% block) were observed (Figure S5). When the potential was dropped back to +50 mV, the activity pattern of αHL-oligoA_1 without aptamerT4 was observed (compare Figure 2b and Figure S5). These results suggest that at high potentials the hybridized DNA is stripped from oligoA.

Aptamer–Thrombin Interactions. After thrombin had been added to the cis chamber, single-channel recordings of αHL-oligoA_1·aptamerT4 pores revealed a new class of events with an increased current amplitude (level UB+T, Figure 3b). These events were not observed when the thrombin was denatured before addition or when bovine albumin serum was used instead (data not shown), which suggests that the events are caused by the interaction of folded thrombin with the attached aptamer. As expected, the addition of excess free aptamers to the cis chamber (after the addition of thrombin) caused a reduction in the frequency of occurrence of the UB+T events (Figure S6). It is not clear why thrombin binding to the aptamer increases the ionic current through the pore. Ion flow could be affected by the presence of charged residues on the surface of the bound thrombin or by a change in the position of the aptamer at the pore entrance caused by thrombin binding. The thrombin binding events have only a minor effect on the ionic current that passes through the pore (~1% increase, Figure 3b). Therefore, a high salt concentration (1 M KCl in both chambers) was used to allow the events to be detected above the noise level. Interestingly, the K_d value for the thrombin·aptamer complex on the nanopore was similar to values obtained at lower salt concentrations with other methods (see below).

The presence of thrombin in the cis chamber also reduced the frequency of the transitions into the B1 level (Figures 3b and S7). Inspection of the recording traces revealed that the transitions into B1 occurred only from the unblocked current

dx.doi.org/10.1021/ja2105653 | J. Am. Chem.Soc. 2012, 134, 2781–2787

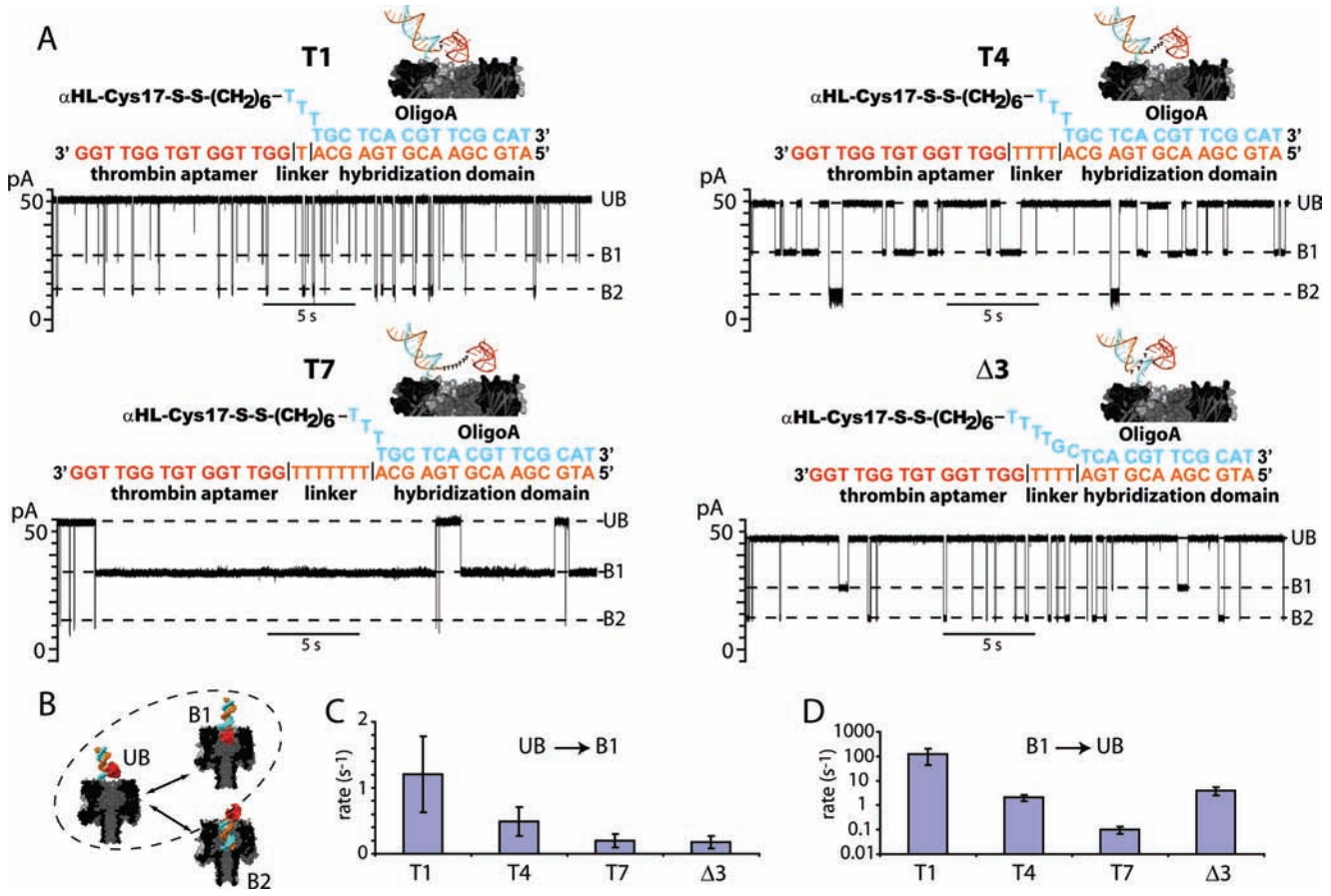

Figure 4. Nature of the linker between the hybridization and the aptamer domains affects aptamer insertion into the pore vestibule. (a) Sequences and representative traces of αHL-oligoA$_1$ pores hybridized with various aptamer oligonucleotides: aptamerT1, aptamerT4, aptamerT7, and aptamerΔ3. The measurements were performed in 1 M KCl, 10 mM Tris.HCl, pH 7.2, at +50 mV. The traces were filtered at 1 kHz. (b) Kinetic model describing the observed transitions. (c) Rates of the transitions from UB to B1. (d) Rates of the transitions from B1 to UB. The models are based on pdb files 7AHL (αHL, gray), 3IAG (dsDNA, light blue and orange), and 148D (thrombin aptamer, red). All measurements were conducted at least 3 times.

level (UB) and not from UB+T (Figure S8). By contrast, transitions into B2 occurred from both UB and UB+T and were not affected by the thrombin binding events (Figure S7 inset, Figure S8). A kinetic model for the transitions between the various currents levels is proposed (Figure 3c). On the basis of this model, the binding of thrombin prevents entry of the aptamer into the pore vestibule (transitions to B1). However, it does not affect entry of the double-stranded domain of the oligoA·aptamerT4 duplex (transitions to B2).

Properties of Various Aptamer Oligonucleotides. In the present approach, different detection units can be quickly coupled to the adapter, oligoA. We took advantage of this to compare the properties of three additional aptamer oligonucleotides. Two have different linkers, with one or seven thymines (aptamerT1 and aptamerT7, respectively) (Figure 4a). The fourth aptamer oligonucleotide (aptamerΔ3) has a 4-nt thymidine linker, but the aptamer has been shifted three nucleotides away from the pore entrance compared to the others by shortening the hybridization domain to 12 nt (Figure 4a). Both B1 and B2 levels were observed for each of the four aptamer oligonucleotides. At a potential of +50 mV, aptamerT1 gives a B1 blockade with a 50 ± 3% current reduction, compared to a ~40% current reduction with the other aptamer oligonucleotides (aptamerT4, 43 ± 1%; aptamerT7, 41 ± 2%; aptamerΔ3, 42 ± 3%). Possibly, the shortest linker restricts the aptamer quadruplex to a smaller volume of the pore vestibule, closer to the entrance, than is allowed by the longer linkers. The frequency of the transitions into current level B1 decreased as the linker length increased (Figure 4c). In addition, the frequency of the events was reduced when the aptamer was shifted away from the pore entrance (aptamerT4 versus aptamerΔ3, Figure 4c). These results suggest that the restriction of the aptamer to the vicinity of the pore entrance with a short linker eases its entry to the pore. The rate of the transition of the aptamer out of the pore (Figure 4d) was slower the longer the linker; the B1 dwell times increased from ~10 ms for aptamerT1, to ~500 ms for aptamerT4, to ~10 000 ms for aptamerT7. Shifting aptamerT4 away from the pore entrance by three nucleotides (aptamerΔ3) reduced the B1 dwell time to ~250 ms. These results suggest that the deeper within the pore the aptamer is located, the longer the period of residence. The linker length and its location did not have a significant influence on the amplitude of the B2 current blockades (Figure S4). This is not surprising, since the B2 blockades are derived from the insertion of duplex DNA into the pore opening, and the amplitude of the block is similar to that found with duplex-forming oligonucleotides without the aptamer sequence (Figures S2a, S3).

Can the three additional aptamer oligonucleotides also sense thrombin binding? In the case of aptamerT1 (Figure S9), a

dx.doi.org/10.1021/ja2105653 | J. Am. Chem.Soc. 2012, 134, 2781−2787

current level was observed similar to that seen with aptamerT4 (UB+T, Figure 3b). However, when thrombin was added to pores carrying aptamerT7 or aptamerΔ3, the differences between the UB and UB+T current levels were harder to distinguish even after filtration of the single-channel recording traces at 50 Hz (Figure S9). In addition, we also positioned the aptamer at the opposite end of the DNA duplex, so that it was located about 4.5 nm away from the pore entrance (Figure S10). In this case, a blockade at about the level of B2 was observed and no thrombin binding events were detected (Figure S10). Therefore, to detect the interactions between the aptamer and thrombin, the aptamer must be restricted to the pore entrance with a carefully adjusted short linker.

Kinetics and Thermodynamics of the Thrombin·Aptamer Interaction. On the basis of the proposed kinetic model (Figure 3c), the rate constants for the aptamer·thrombin interactions were determined for aptamerT1 and aptamerT4, by observing the transitions between the UB and UB+T levels at different thrombin concentrations, and found to be similar (Figure 5). The association rate constants were k_{on} = 1.20 ± 0.14 × 10^7 M^{-1} s^{-1} (n = 3) for aptamerT1 and k_{on} = 1.97 ± 0.01 × 10^7 M^{-1} s^{-1} (n = 4) for aptamerT4. The dissociation rate constants were k_{off} = 1.5 ± 0.2 s^{-1} (n = 3) for aptamerT1 and k_{off} = 1.5 ± 0.1 s^{-1} (n = 4) for aptamerT4. These results also give us information about the sensor sensitivity. At the lowest thrombin concentration tested (20 nM), aptamer·thrombin interactions occur at about 2 s^{-1} (Figure 5); i.e., we can assay thrombin, a model protein in the present approach, at low nM concentrations in as little as a few minutes.

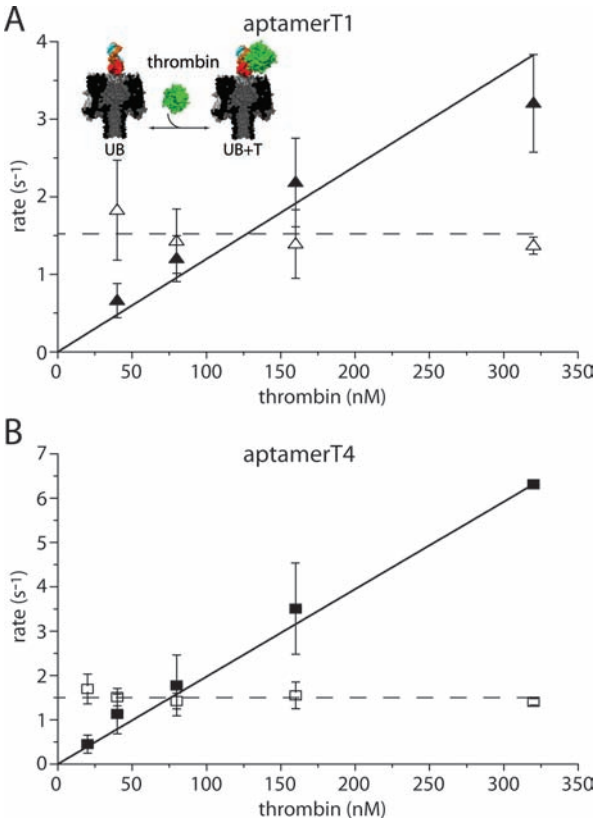

Figure 5. Dependence of the rates of the transitions between the UB and UB+T current levels on thrombin concentration. (a) AptamerT1, triangles; (b) aptamerT4, squares. Association rates, filled symbols; dissociation rates, empty symbols. The rates were calculated with QuB on the basis of the kinetic model (Figure 3b). The measurements were performed in 1 M KCl, 10 mM Tris.HCl, pH 7.2, at +50 mV, and were conducted at least 3 times.

On the basis of the rate constants found for aptamerT4 and aptamerT1, equilibrium dissociation constants of K_d = 77 ± 6 nM and K_d = 126 ± 34 nM were calculated. These values are similar to K_d values for the thrombin·aptamer interaction determined previously by other approaches (20–450 nM).[29,36–41] The kinetics of the thrombin·aptamer interaction have been determined by surface plasmon resonance (SPR), where the binding of free thrombin to a biotinylated aptamer immobilized on a streptavidin-coated surface was measured,[42–44] and by various capillary electrophoresis (CE) techniques[38,41] (Table S1). These results gave a wide range of values (Table S1). Single-molecule measurements of ligand·analyte interactions with nanopores have some advantages over these ensemble techniques. For example, the measurements do not suffer from steric hindrance due to crowding of the binding sites, which can occur on the surface of an SPR chip.[45] Further, in the nanopore approach, the detector is functional only when an active ligand is attached to the nanopore. By comparison, in ensemble measurements, it is common to have a mixture of active and inactive ligands in an unknown ratio (for example, see Gong et al.[41]). In addition, in the technique presented here, the analyte·ligand interaction occurs in a static chamber; it is not dependent on a molecular flow rate, which can bias the measurement accuracy in SPR and CE. For example, when the analyte flow rate in SPR is too slow, an analyte molecule can rebind to the chip surface and as a result complicate the analysis of the interaction kinetics.[45]

■ CONCLUSIONS

We have demonstrated that a protein nanopore equipped with a DNA adapter can be hybridized with various oligonucleotides that have different properties. Therefore, the same nanopore construct might be used to detect different analytes, depending on the detection unit that is hybridized to it. By contrast, when the detection unit is directly covalently attached to the nanopore,[15–17] a sensor for each analyte must be made separately in a more laborious fashion. With the development of new approaches for building bilayer[46–48] and nanopore[49] arrays, it will be possible to build arrays of nanopores modified with DNA adapters attached to different detection units for the parallel detection of a variety of analytes in a single sample.

■ ASSOCIATED CONTENT

Supporting Information

Materials and methods details, a table, and 10 figures. This material is available free of charge via the Internet at http://pubs.acs.org

■ AUTHOR INFORMATION

Corresponding Author

hagan.bayley@chem.ox.ac.uk

Present Address

[§]Institute of Chemistry, The Hebrew University of Jerusalem, 91904 Israel.

■ ACKNOWLEDGMENTS

This study was supported by the MRC, Oxford Nanopore Technologies, and the European Commission's seventh Framework

Programme (FP7) READNA Consortium. We thank Dr. Stephen Cheley for plasmids.

REFERENCES

(1) Bayley, H.; Martin, C. R. *Chem. Rev.* **2000**, *100*, 2575−2594.
(2) Bayley, H.; Cremer, P. S. *Nature* **2001**, *413*, 226−230.
(3) Dekker, C. *Nat. Nanotechnol.* **2007**, *2*, 209−15.
(4) Sexton, L. T.; Horne, L. P.; Martin, C. R. *Mol. Biosyst.* **2007**, *3*, 667−85.
(5) Howorka, S.; Siwy, Z. *Chem. Soc. Rev.* **2009**, *38*, 2360−84.
(6) Siwy, Z. S.; Howorka, S. *Chem. Soc. Rev.* **2010**, *39*, 1115−32.
(7) Majd, S.; Yusko, E. C.; Billeh, Y. N.; Macrae, M. X.; Yang, J.; Mayer, M. *Curr. Opin. Biotechnol.* **2010**, *21*, 439−476.
(8) Braha, O.; Gu, L.-Q.; Zhou, L.; Lu, X.; Cheley, S.; Bayley, H. *Nat. Biotechnol.* **2000**, *17*, 1005−1007.
(9) Hammerstein, A. F.; Shin, S. H.; Bayley, H. *Angew. Chem., Int. Ed.* **2010**, *49*, 5085−5090.
(10) Braha, O.; Walker, B.; Cheley, S.; Kasianowicz, J. J.; Song, L.; Gouaux, J. E.; Bayley, H. *Chem. Biol.* **1997**, *4*, 497−505.
(11) Gu, L.-Q.; Braha, O.; Conlan, S.; Cheley, S.; Bayley, H. *Nature* **1999**, *398*, 686−690.
(12) Cheley, S.; Gu, L.-Q.; Bayley, H. *Chem. Biol.* **2002**, *9*, 829−838.
(13) Shin, S.-H.; Luchian, T.; Cheley, S.; Braha, O.; Bayley, H. *Angew. Chem., Int. Ed.* **2002**, *41*, 3707−3709.
(14) Howorka, S.; Cheley, S.; Bayley, H. *Nat. Biotechnol.* **2001**, *19*, 636−639.
(15) Movileanu, L.; Howorka, S.; Braha, O.; Bayley, H. *Nat. Biotechnol.* **2000**, *18*, 1091−1095.
(16) Howorka, S.; Nam, J.; Bayley, H.; Kahne, D. *Angew. Chem., Int. Ed.* **2004**, *43*, 842−846.
(17) Xie, H.; Braha, O.; Gu, L.-Q.; Cheley, S.; Bayley, H. *Chem. Biol.* **2005**, *12*, 109−120.
(18) Cheley, S.; Xie, H.; Bayley, H. *ChemBioChem* **2006**, *7*, 1923−1927.
(19) Howorka, S.; Movileanu, L.; Braha, O.; Bayley, H. *Proc. Natl. Acad. Sci. U.S.A.* **2001**, *98*, 12996−13001.
(20) Howorka, S.; Bayley, H. *Biophys. J.* **2002**, *83*, 3202−3210.
(21) Wilson, D. S.; Szostak, J. W. *Annu. Rev. Biochem.* **1999**, *68*, 611−47.
(22) Shamah, S. M.; Healy, J. M.; Cload, S. T. *Acc. Chem. Res.* **2008**, *41*, 130−8.
(23) Cho, E. J.; Lee, J. W.; Ellington, A. D. *Annu. Rev. Anal. Chem.* **2009**, *2*, 241−64.
(24) Nimjee, S. M.; Rusconi, C. P.; Sullenger, B. A. *Annu. Rev. Med.* **2005**, *56*, 555−83.
(25) Tuerk, C.; Gold, L. *Science* **1990**, *249*, 505−10.
(26) Ellington, A. D.; Szostak, J. W. *Nature* **1990**, *346*, 818−22.
(27) Tombelli, S.; Minunni, M.; Mascini, M. *Biosens. Bioelectron.* **2005**, *20*, 2424−34.
(28) Ding, S.; Gao, C.; Gu, L. Q. *Anal. Chem.* **2009**, *81*, 6649−55.
(29) Bock, L. C.; Griffin, L. C.; Latham, J. A.; Vermaas, E. H.; Toole, J. J. *Nature* **1992**, *355*, 564−6.
(30) Macaya, R. F.; Schultze, P.; Smith, F. W.; Roe, J. A.; Feigon, J. *Proc. Natl. Acad. Sci. U.S.A.* **1993**, *90*, 3745−9.
(31) Padmanabhan, K.; Padmanabhan, K. P.; Ferrara, J. D.; Sadler, J. E.; Tulinsky, A. *J. Biol. Chem.* **1993**, *268*, 17651−4.
(32) Wang, K. Y.; McCurdy, S.; Shea, R. G.; Swaminathan, S.; Bolton, P. H. *Biochemistry* **1993**, *32*, 1899−904.
(33) Gouaux, J. E.; Braha, O.; Hobaugh, M. R.; Song, L.; Cheley, S.; Shustak, C.; Bayley, H. *Proc. Natl. Acad. Sci. U.S.A.* **1994**, *91*, 12828−12831.
(34) Shim, J. W.; Gu, L. Q. *J. Phys. Chem. B* **2008**, *112*, 8354−60.
(35) Shim, J. W.; Tan, Q.; Gu, L. Q. *Nucleic Acids Res.* **2009**, *37*, 972−82.
(36) Macaya, R. F.; Waldron, J. A.; Beutel, B. A.; Gao, H.; Joesten, M. E.; Yang, M.; Patel, R.; Bertelsen, A. H.; Cook, A. F. *Biochemistry* **1995**, *34*, 4478−92.
(37) German, I.; Buchanan, D. D.; Kennedy, R. T. *Anal. Chem.* **1998**, *70*, 4540−5.
(38) Berezovski, M.; Nutiu, R.; Li, Y.; Krylov, S. N. *Anal. Chem.* **2003**, *75*, 1382−6.
(39) Huang, C. C.; Cao, Z.; Chang, H. T.; Tan, W. *Anal. Chem.* **2004**, *76*, 6973−81.
(40) Muller, J.; Wulffen, B.; Potzsch, B.; Mayer, G. *ChemBioChem* **2007**, *8*, 2223−6.
(41) Gong, M.; Nikcevic, I.; Wehmeyer, K. R.; Limbach, P. A.; Heineman, W. R. *Electrophoresis* **2008**, *29*, 1415−22.
(42) Hasegawa, H.; Taira, K.-i.; Sode, K.; Ikebukuro, K. *Sensors* **2008**, *8*, 1090−1098.
(43) Ostatna, V.; Vaisocherova, H.; Homola, J.; Hianik, T. *Anal. Bioanal. Chem.* **2008**, *391*, 1861−9.
(44) Pinto, A.; Bermudo Redondo, M. C.; Ozalp, V. C.; O'Sullivan, C. K. *Mol. Biosyst.* **2009**, *5*, 548−53.
(45) Myszka, D. G. *Curr. Opin. Biotechnol.* **1997**, *8*, 50−7.
(46) Baaken, G.; Sondermann, M.; Schlemmer, C.; Ruhe, J.; Behrends, J. C. *Lab Chip* **2008**, *8*, 938−44.
(47) Syeda, R.; Holden, M. A.; Hwang, W. L.; Bayley, H. *J. Am. Chem. Soc.* **2008**, *130*, 15543−15548.
(48) Osaki, T.; Suzuki, H.; Le Pioufle, B.; Takeuchi, S. *Anal. Chem.* **2009**, *81*, 9866−70.
(49) Hall, A. R.; Scott, A.; Rotem, D.; Mehta, K. K.; Bayley, H.; Dekker, C. *Nat. Nanotechnol.* **2010**, *5*, 874−877.